Synergistic Effect of Phosphorus-Containing Nanosponges on Intumescent Flame-Retardant Polypropylene

Xuejun Lai, Xingrong Zeng, Hongqiang Li, Changyu Yin, Haili Zhang, Feng Liao

College of Materials Science and Engineering, South China University of Technology, Guangzhou 510640, China

Received 5 August 2011; accepted 20 September 2011
DOI 10.1002/app.35646
Published online 17 January 2012 in Wiley Online Library (wileyonlinelibrary.com).

ABSTRACT: A novel nanosponge (NS) was synthesized via the crosslinking of β-cyclodextrin with epoxy resin. Subsequently, a phosphorus-containing nanosponge (P–NS) was prepared by the absorbance of resorcinol bis(diphenyl phosphate) into the NS, and it was used as a synergistic agent of intumescent flame retardance in a polypropylene (PP)/melamine pyrophosphate/pentaerythritol composite. The synergistic effect between P–NS and the intumescent flame retardant (IFR) was investigated by thermogravimetry, limiting oxygen index (LOI) testing, vertical burning (UL-94) testing, cone calorimeter testing, and scanning electron microscopy (SEM). The results show that P–NS significantly improved the flame retardancy of the PP/IFR composite. When 3.0 wt % P–NS replaced the same amount of IFR in the composite, the LOI value increased from 29.0 to 32.5%, the UL-94 rating was enhanced from V-1 to V-0, and the peak heat release rate decreased substantially from 343 to 235 kW/m^2. Simultaneously, the total heat release and mass loss rate decreased dramatically. Furthermore, the SEM results show that the quality of char formation of the PP/IFR/P–NS was superior to that of the PP/IFR composite. © 2012 Wiley Periodicals, Inc. J Appl Polym Sci 125: 1758–1765, 2012

Key words: composites; flame retardance; intumescence; poly(propylene) (PP); polyolefins

INTRODUCTION

Polypropylene (PP) is one of the most important plastics and is widely used in many fields. However, its further application is severely limited by its flammability and burning with dripping. Therefore, it is imperative to improve the flame retardancy of PP. In recent years, research in halogen-free flame retardants (FRs) has attracted more and more attention because of the possible environment and health hazards posed by the use of halogen FRs.[1] Among various halogen-free FRs, intumescent flame retardants (IFRs) are remarkable because of their low toxic smog and antidripping.[2,3] Generally, a typical IFR system is composed of three basic ingredients: a char-forming agent, an acid catalyst, and a blowing source.[3] When heated beyond a critical temperature, the IFR system generates a swollen multicellular char, which acts as a physical barrier, which slows down heat and mass transfer between the gas and condensed phases and, thus, protects the substrate material from burning.[1,3] Nevertheless, IFR's relatively low flame retardancy impedes its actual application. To enhance its FR efficiency, many synergists have been introduced into the system, including sepiolite,[4,5] vermiculite,[6] fumed silica,[7] iron powder,[8] metal oxides,[9] nickel phosphates,[10] zeolites,[2,11] and montmorillonite.[12,13] Recently, the development of new synergists for IFR has become a hot issue.

Resorcinol bis(diphenyl phosphate) (RDP), as an aryl phosphate ester possessing a high phosphorus content (ca. 10.7 wt %) and good thermal stability, was found to be a superior FR for engineering plastics, such as polycarbonate/acrylonitrile-butadiene-styrene blends.[14,15] It has good potential for enhancing the flame retardancy of PP/IFR composites. However, as a viscous liquid, RDP is difficult to incorporate and retain in solid polymer composites.[16] We suggest that this issue can be solved via the absorbance of RDP into nanosponges (NSs) synthesized by the crosslinking of β-cyclodextrin (β-CD) with epoxy. β-CD, consisting of seven glucopyranose units, has been proven to be a good charring agent.[17,18] Besides, it is well-known for forming an inclusion complex with various guest molecules because of its special molecular structures: a hydrophobic internal cavity and a hydrophilic external surface.[16,19,20] Through the reaction of β-CD with suitable crosslinking agents, a novel nanostructure material, NS, can be obtained.[21,22] Because of its outstanding encapsulation capacity, NSs can adsorb a great variety of substances.[21,23] As a result, they can be used as an efficient carrier for liquid FRs, including RDP. We propose that the phosphorus-containing nanosponge (P–NS) would show a good synergistic effect with IFR in FR PP.

In this study, P–NS was prepared by the absorbance of RDP into NS synthesized by the crosslinking of β-CD with epoxy resin. The P–NS was then

Correspondence to: X. Zeng (psxrzeng@gmail.com).

combined with IFR to flame-retard PP, and their synergistic effect was investigated. The structures of NS and P–NS were characterized by Fourier transform infrared (FTIR) spectroscopy. The thermal properties and flammability of the FR PP were investigated by thermogravimetry (TG), limiting oxygen index (LOI) testing, vertical burning (UL-94) testing, and cone calorimeter testing (CCT). The char residue after CCT was examined by scanning electron microscopy (SEM).

EXPERIMENTAL

Materials

β-CD powder was obtained from Shanghai Bio Science & Technology Co., Ltd. (Shanghai Municipality, China). Epoxy resin (E-51, liquid diglycidyl ether of bisphenol A, containing 5.1 mmol epoxy groups/g of resin) was purchased from Guangzhou Dongfeng Chemical Industrial Co., Ltd. (Guangdong Province, China). RDP (a colorless, clear, viscous liquid with a phosphorous content of 10.7 wt %) was provided by Jiangsu Yoke Technology Co., Ltd. (Jiangsu Province, China). PP [T30S, a granulated product with a melt flow index of 3.0 g/10 min (230°C, 2.16 kg)] was provided by Maoming Petrochemical Co., Ltd. (Guangdong Province, China). Melamine pyrophosphate (MPP) powder (average particle size < 0.12 mm) was obtained from Jiangmen Topchem Technology Co., Ltd. (Guangdong Province, China). Pentaerythritol (PER) powder (average particle size < 0.12 mm) was purchased from Tianjin Kermel Chemical Reagent Co., Ltd. (Tianjin Municipality, China). Antioxidant (B215) was provided by Ciba Specialty Chemicals, Inc. (Basel, Switzerland). All these commercial materials were used directly without further purification.

Synthesis of the NS

β-CD (0.3 mol) and NaOH (0.3 mol) were added to a 500-mL, round-bottom flask containing 200 mL of distilled water and stirred at 80°C until a transparent mixture was formed. Epoxy resin E-51 (0.3 mol) was dissolved in 100 mL of dimethyl sulfoxide, and the mixture was added dropwise to the β-CD solution. The mixture was stirred at 80°C for 6 h. Subsequently, the solid obtained was precipitated and washed with a large excess of hot water and ethanol to remove unreacted β-CD and the E-51 byproduct. Finally, the solid was ground in a mortar and dried at 80°C *in vacuo*, and the NS was obtained. The reaction scheme and structure of the NS are shown in Figure 1.

Preparation of P–NS

NS (20.0 g) was added to a 500-mL, round-bottom flask containing 200 mL of ethanol and stirred at 70°C for 4 h until a homogeneous mixture was formed. RDP (10.0 g) was dissolved in 50 mL of ethanol, and the mixture was added dropwise to the NS suspension. The mixture was stirred at 75°C for 4 h. Afterward, the solution was precipitated, filtered, and dried in a vacuum oven at 100°C for 24 h. The dried product was crushed into a fine powder, and P–NS was obtained.

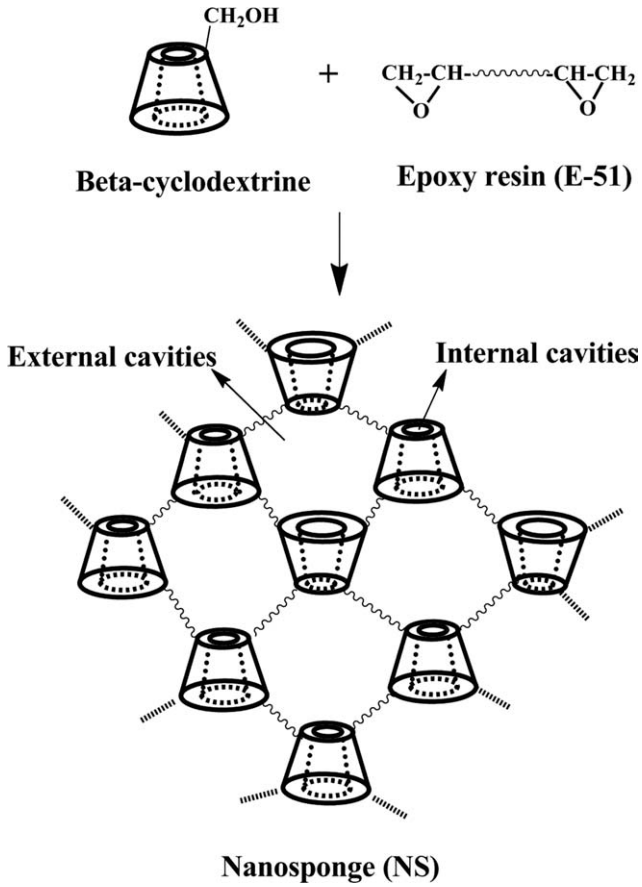

Figure 1 Reaction scheme and the structure of NS.

Preparation of the flame-retardant PP

MPP and PER were melt-mixed with PP on a two-roll mill (XK-160, Changzhou Shuangfeng Machinery Factory, Jiangsu Province, China) at 170°C for 10 min. Then, the P–NSs were added to the PP/IFR composite and mixed for another 10 min, and FR PP was prepared, with the total content of FR (IFR + P–NS) kept at 25 wt %. The prepared composites were hot-pressed into sheets of suitable thickness and size for the corresponding tests.

Characterization

Fourier transform infrared (FTIR) spectroscopy

The samples were mixed with KBr powder, and the mixture was pressed into a tablet. The FTIR spectra of the samples were recorded with a Tensor 27 spectrometer (Bruker Optics, Karlsruhe, Germany). The

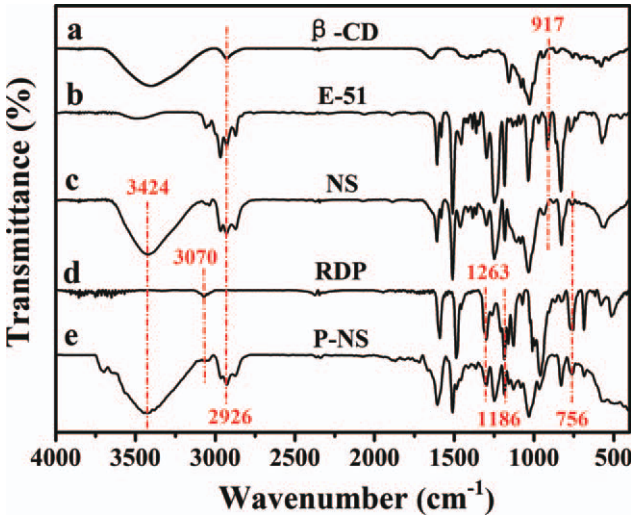

Figure 2 FTIR spectra of β-CD, E-51, NS, RDP, and P–NS. [Color figure can be viewed in the online issue, which is available at wileyonlinelibrary.com.]

measurements were carried out in the range 4000–400 cm^{-1}.

Thermogravimetric analysis

Thermogravimetric analysis was carried out with a thermogravimeter (TG209, Netzsch Instruments Co., Selb, Germany) from 30 to 700°C at a linear heating rate of 20°C/min under an air atmosphere.

LOI testing

The LOI test was carried out with an oxygen index meter (HC-2, Jiangning Analysis Instrument Co., Jiangsu Province, China) according to ASTM D 2863-2008. The dimensions of the specimens were 120 × 6.5 × 3 mm^3.

UL-94 testing

The UL-94 test was conducted on a vertical burn instrument (CFZ-3, Jiangning Analysis Instrument Co., Jiangsu Province, China) according to ASTM D 635-2003. The dimensions of the specimens were 127 × 12.7 × 3.2 mm^3.

CCT

CCT was carried out with a cone calorimeter (Fire Testing Technology Ltd., West Sussex, UK) according to ISO5660. Each specimen, with dimensions of 100 × 100 × 4 mm^3, was wrapped in aluminum foil and exposed horizontally to an external heat flux of 35 kW/m^2. All tests were run in duplicate, and the average value is reported. The residue of FR PP after the test was photographed by a digital camera (PowerShot A2000 IS, Canon Inc., Utsunomiya, Japan).

SEM

The upper and lower surfaces of the char residue of FR PP after CCT was observed by a scanning electron microscope (JSM-6380, JEOL Ltd., Tokyo, Japan) with an accelerating voltage of 15 kV. The residue was coated with a gold layer before observation.

RESULTS AND DISCUSSION

FTIR analysis

Figure 2(a–e) shows the FTIR spectra of β-CD, E-51, NS, RDP, and P–NS, respectively. For β-CD, the bands at 3398 and 2926 cm^{-1} were assigned to the stretching vibration of O—H and C—H, respectively; the absorption peak at 1028 cm^{-1} was attributed to the stretching vibration of C—O, and the peak at 1158 cm^{-1} was from the antisymmetric stretching vibration of the C—O—C glycosidic bridge.[24–26] The FTIR spectrum of E-51 was characterized by the epoxide group peak located at 917 cm^{-1}.[27] After reaction with β-CD, the band ascribed to the epoxy ring disappeared completely; this was in agreement with the breakage of the ring by the alcoholate of β-CD. Meanwhile, the other bands characteristic for β-CD and E-51 were presented in the corresponding product [as shown in Fig. 2(c)]; this indicated that the NS was successfully synthesized. In the spectrum of RDP, the bands located at 3070 and 1589 cm^{-1} were characteristic of aryl —CH_2 stretching and aryl C=C stretching; the bands at 1263, 1186, 1010, and 756 cm^{-1} were attributed to P=O, P—O—Ar, and P—O—C stretching, respectively.[15,28,29] The spectrum of P–NS still presented the O—H and —CH_2 groups of NS and the characteristic groups of RDP (aryl —CH_2, P—O—Ar, and P—O—C). The results indicate that RDP was trapped in the NS cavities.

LOI measurement and UL-94 rating

As is well known, LOI measurement and UL-94 testing are two widely used approaches for evaluating the flammability of materials. The effects of the P–NS content on the LOI values and UL-94 rating of the FR PP are presented in Table I. As can be seen, the LOI value of the PP/IFR composite without P–NS was 29.0%. When part of the IFR was substituted by P–NS, the flame retardancy of the composite was improved. The LOI values initially increased with increasing P–NS content until a maximum LOI value of 32.5% was reached at 2.0 wt %, but with further increases in the P–NS content, the LOI value decreased. In the vertical burning testing, a V-1 rating in the UL-94 standard was observed when the PP/IFR contained no P–NS. However, when even a

TABLE I
Effects of the P–NS Content on the LOI Values and UL94 Ratings of FR PP

Content of P–NS (wt%)	LOI (%)	UL-94 rating
0	29.0	V-1
0.5	30.5	V-0
1.0	31.5	V-0
2.0	32.5	V-0
3.0	32.0	V-0
4.0	30.5	V-1
6.0	28.5	No rating

PP/IFR/P–NS = $75/(25 - x)/x$, where x is the content of P–NS; IFR: MPP/PER = 3 : 1 w/w.

small amount (0.5 wt %) of P–NS was added to the PP/IFR composite, it effectively prevented dripping, and the UL-94 rating was improved from V-1 to V-0. This could be explained by the fact that the RDP absorbed in P–NS contained a high amount of phosphorus. When combusted, RDP generated phosphinic acid, which was beneficial to the formation of a network structure by esterification, enhanced the char formation, and made the formed char more compact and dense, thus improving the flame retardancy.[15,30] However, an excessive P–NS content decreased the flame retardancy of the composite. This was because P–NS acted as a catalyst in the PP/IFR composite for char formation. When P–NS was more than 2.0 wt %, the esterification speed of the system did not match the foaming speed well; this destroyed the char swelling behavior of the composite and resulted in an unsatisfactory flame retardancy.[18,31] Therefore, on the basis of the results of the LOI and UL-94 tests, an appropriate P–NS content of 2.0 wt % was optimum for the flame retardancy.

TABLE II
TG Characteristic Parameters of PP and FR PP

Sample	T_{onset} (°C)	T_{max} (°C)	R_{max} (%/min)	Residue at 700°C (wt %)
PP	264	339	14	0
PP/IFR	279	343	10.8	4.8
PP/IFR/P–NS (2 wt %)	268	$T_1 = 353$, $T_2 = 396$	$R_1 = 7.7$, $R_2 = 6.5$	7.3

Thermal decomposition behavior

Figure 3 shows the TG and DTG curves of PP, PP/IFR, and PP/IFR/P–NS in an air atmosphere. The onset decomposition temperature (T_{onset}) is defined as the temperature at which a 5% mass loss occurs. The relative thermostability of the samples was evaluated by the T_{onset}, maximum rate decomposition temperature (T_{max}), maximum mass loss rate (R_{max}), and percentage of residue at 700°C. The corresponding characteristic parameters are presented in Table II. The pure PP showed one weight-loss stage in the range 260–360°C, and it left no residual char at 700°C. As for the PP/IFR composite, it exhibited similar thermal decomposition behavior to that of PP. However, it was observed that more residual char was obtained for the PP/IFR samples than for pure PP. Moreover, T_{onset} and T_{max} of the PP/IFR composite were 279 and 343°C; these values were 15 and 4°C higher than those of the PP resin, respectively. This was primarily attributed to the formation of the intumescent char, which protected the substrate material from decomposing.[4,12] In comparison with the PP/IFR composite, the PP/IFR/P–NS composite showed a different thermal decomposition behavior. T_{onset} of the PP/IFR/P–NS composite was 11°C lower than that of PP/IFR, and two main

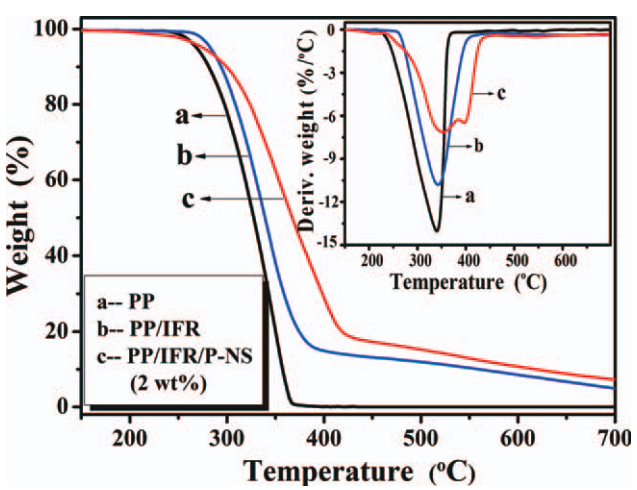

Figure 3 TG and DTG curves of PP, PP/IFR, and PP/IFR/P–NS in air. [Color figure can be viewed in the online issue, which is available at wileyonlinelibrary.com.]

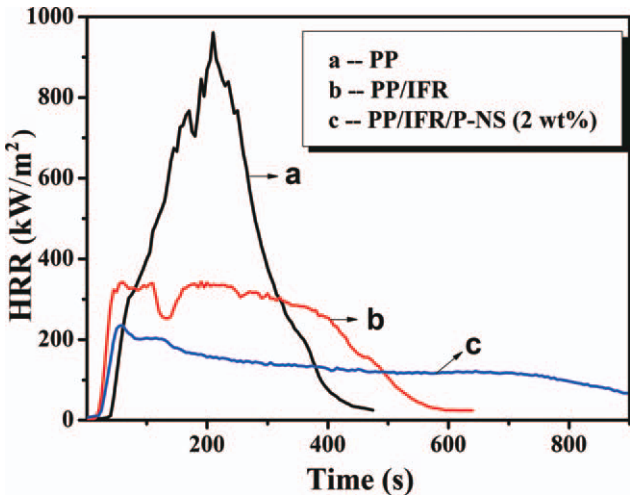

Figure 4 HRR curves of PP and the FR PP at a flux of 35 kW/m^2. [Color figure can be viewed in the online issue, which is available at wileyonlinelibrary.com.]

TABLE III
Combustion Parameters of PP and the FR PP

Sample	TTI (s)	PHRR (kW/m^2)	av-HRR (kW/m^2)	THR (MJ/m^2)	av-MLR (g s^{-1}·m^2)	FPI (m^2·s kW^{-1})
PP	54	961	403	175	0.043	0.056
PP/IFR	32	343	190	136	0.027	0.093
PP/IFR/P–NS (2 wt %)	30	235	128	118	0.018	0.166

stages of decomposition were observed, as shown in Figure 3(c). The first stage occurred roughly from 250 to 385°C and was ascribed to the char-forming reaction and decomposition of the composite; the second stage was probably due to the destruction of the protective layer.[18] The T_{max} values of the two stages were 353 and 396°C; these values were 10 and 53°C higher than those of the PP/IFR composite, respectively. Meanwhile, with the incorporation of IFR and P–NS, R_{max} of the composite decreased from 14 to 7.7%/min. Furthermore, a higher residue yield of the PP/IFR/P–NS sample at 700°C was observed. The results mentioned previously indicate that P–NS accelerated the esterification and dehydrated carbonization of IFR and promoted the char-forming performance of the PP/IFR composite.

Cone calorimeter analysis

CCT is used for the bench-scale assessment of combustion performance. Various parameters can be obtained from the test,[32] including the time to ignition (TTI), heat release rate (HRR), average heat release rate (av-HRR), total heat release (THR), average mass loss rate (av-MLR), and fire performance index [FPI; defined as the ratio of TTI to the peak heat release rate (PHRR)]. HRR has been recognized as one of the most important parameters for characterizing a fire. An effective FR system normally shows a low HRR value.[5] Figure 4 shows the HRR curves of PP and FR PP. The pure PP burned rapidly after ignition, and HRR reached a sharp peak (PHRR) of 961 kW/m^2, whereas PHRR of PP/IFR was 343 kW/m^2, which was reduced by 64.3%. With the addition of 2 wt % P–NS, the PHRR of FR PP was further reduced to 235 kW/m^2; this indicated that the synergistic effect of IFR and P–NS improved the flame retardancy of the composite, whereas there was a decrease in TTI with the addition of IFR and P–NS (as shown in Table III). This could be explained by the fact that the temperature of the composite surfaces increased more quickly because the presence of the solidlike intumescent layer prevented effective heat transfer.[33]

Figures 5 and 6 show the THR and mass loss rate (MLR) curves of PP and FR PP, respectively. The corresponding characteristic parameters are presented in Table III. Similar conclusions were drawn, that the THR, MLR, and av-MLR decreased with the incorporation of IFR and IFR/P–NS. These results illustrate a good synergistic effect between IFR and P–NS in PP. FPI is independent of the dimensions of samples and is used to evaluate the fire danger of materials.[34] The bigger the FPI value is, the smaller the fire danger is (i.e., the time to flash burning is longer).[35] As presented in Table III, PP/IFR/P–NS had the biggest FPI value of 0.166 m^2·s/kW; again, this indicated that P–NS efficiently improved the flame retardancy of the PP/IFR composite.

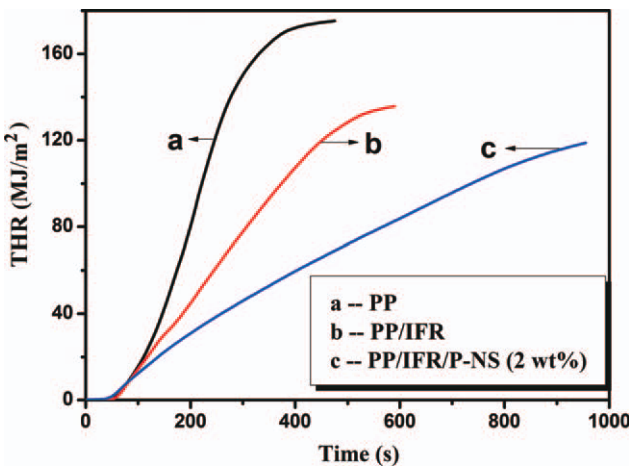

Figure 5 THR curves of PP and FR PP at a flux of 35 kW/m^2. [Color figure can be viewed in the online issue, which is available at wileyonlinelibrary.com.]

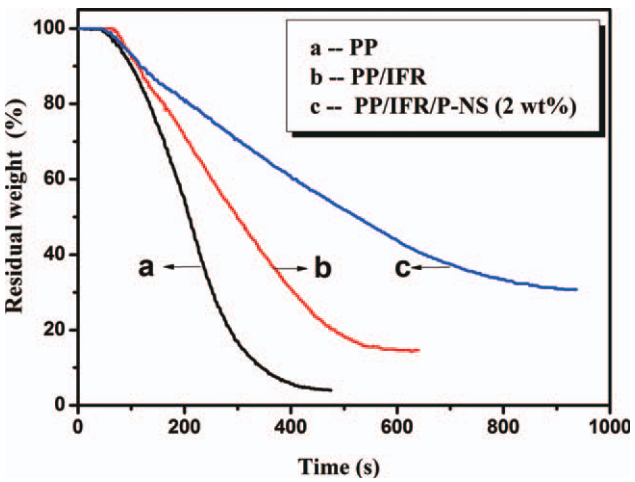

Figure 6 MLR curves of PP and FR PP at a flux of 35 kW/m^2. [Color figure can be viewed in the online issue, which is available at wileyonlinelibrary.com.]

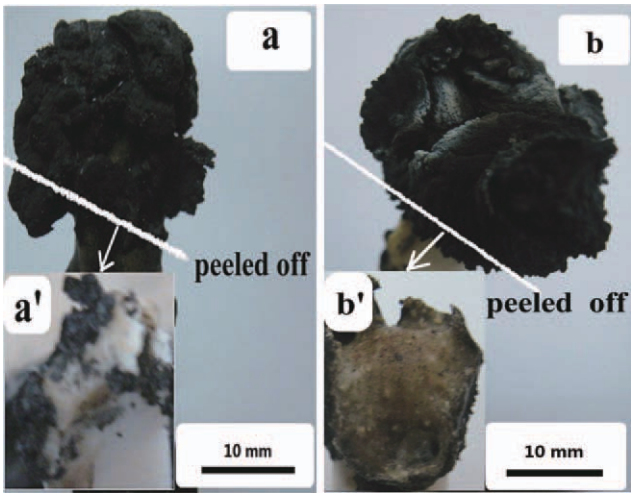

Figure 7 Digital photographs of the char residue for FR PP after the LOI test: (a) PP/IFR, (b) PP/IFR/P–NS (2 wt %), (a′) peeled PP/IFR, and (b′) peeled PP/IFR/P–NS (2 wt %). The total content of IFR and P–NS was 25 wt %. [Color figure can be viewed in the online issue, which is available at wileyonlinelibrary.com.]

Morphology of the residual char

To further clarify the FR mechanism, the morphology of the residual char for the composites was observed. The digital photographs of the char residue for the FR PP after the LOI test is shown in Figure 7. The intumescent char residue of the PP/IFR composite was rather fluffy, and the char layer could be easily peeled off of the substrate. As shown in Figure 7(a′), the cross section between the char layer and the PP matrix was white and smooth; this indicated that the interface between the char layer and the substrate material had little or no transition layer, and the cohesion between the char layer and the substrate material was weak.[36] Accordingly, the inferior quality of the char residue led to the unsatisfied flame retardancy of the PP/IFR composite. Fortunately, the quality of the char residue was improved by the incorporation of P–NS. As shown in Figure 7(b), the char layer of the PP/IFR/P–NS composite was compact and could be hardly peeled off of the substrate. Meanwhile, the cross section between the char layer and PP matrix was yellow and rough [see Fig. 7(b′)]. This indicated that the PP/IFR/P–NS composite easily formed a compact and dense char layer to prevent heat and gas transfer; this improved the flame retardancy of the composite.

Figure 8 shows the digital photographs of the char residue for FR PP after CCT. As shown in Figure 8(a), the surface of the PP/IFR residue was covered with an expanded char network, but it was thin and broken up during combustion. Consequently, the barrier could not effectively prevent both heat and mass transfer. With the addition of 2.0 wt % P–NS, the char was more dense and compact in comparison with PP/IFR. This further confirmed the synergistic effect between P–NS and IFR in enhancing char formation for the PP resin.

The morphology of the residual char formed after CCT was also investigated by SEM. Figure 9(A_1, A_2, B_1,B_2) presents the SEM photographs of the upper and lower char surfaces of the PP/IFR and PP/IFR/P–NS composites, respectively. From Figure 9(A_1,A_2), relatively loose structures including cracks and cavities on the upper surface and some incomplete hollow fractured char on the lower surface were observed in the PP/IFR composite, so it could not effectively protect the underlying material from burning. This might have been the primary reason for its poor flame retardancy. In the presence of 2 wt % P–NS, the upper and lower char surfaces of the FR PP were more compact and dense, as shown in Figure 9(B_1,B_2); again, this indicated

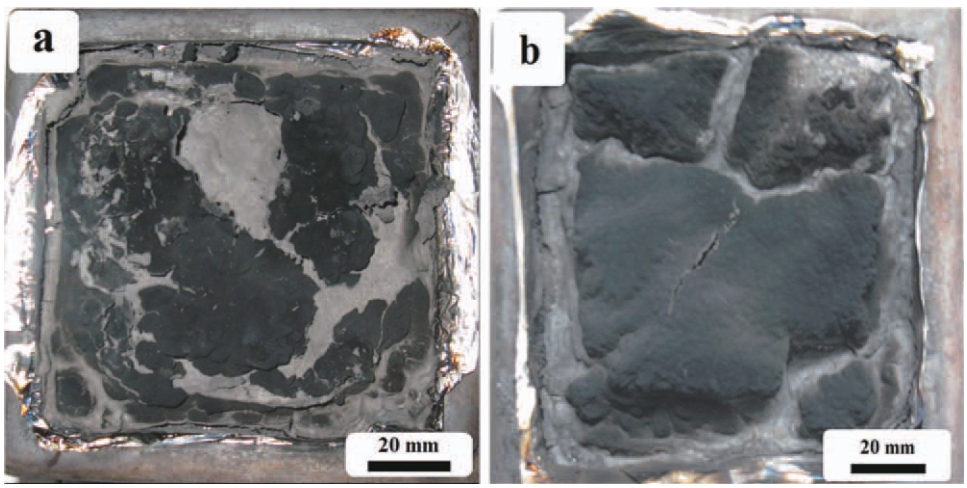

Figure 8 Digital photographs of the char residue for FR PP after CCT: (a) PP/IFR and (b) PP/IFR/P–NS (2 wt %). The total content of IFR and P–NS was 25 wt %. [Color figure can be viewed in the online issue, which is available at wileyonlinelibrary.com.]

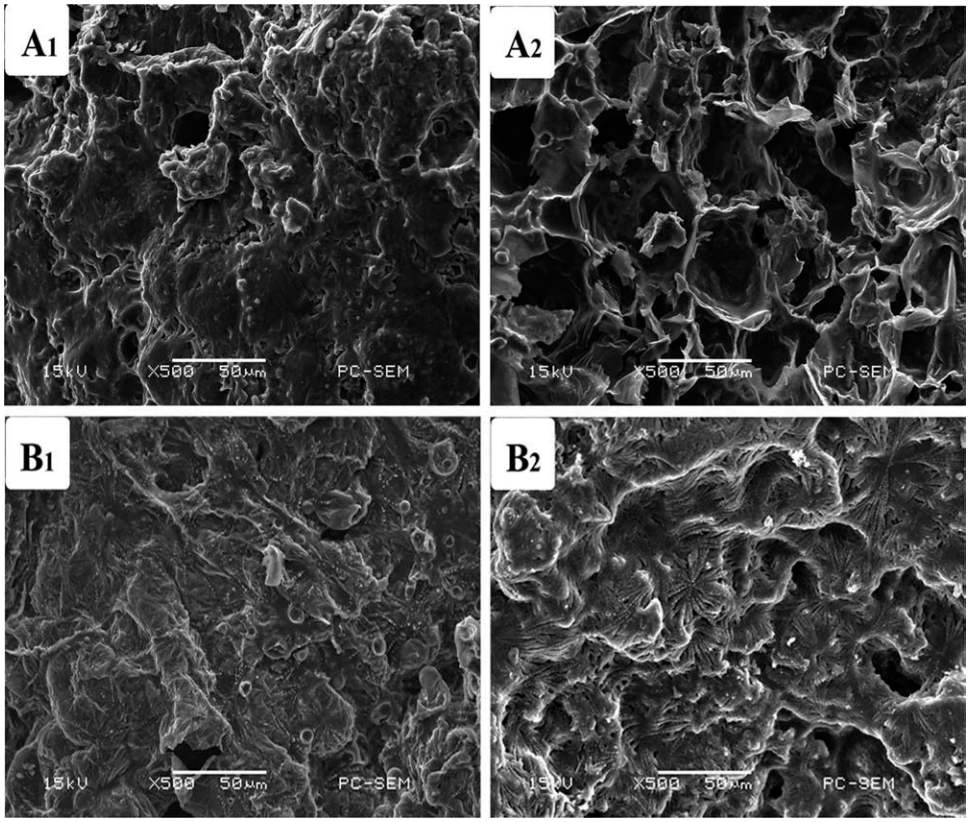

Figure 9 Scanning electron micrographs of the (A_1,B_1) upper surface and (A_2,B_2) the lower surface of the intumescent char obtained from the samples after CCT: (A) did not contain P–NS in the PP/IFR and (B) contained 2 wt % P–NS in the PP/IFR.

that P–NS had a good synergistic effect with IFR on char formation.

CONCLUSIONS

P–NS consisting of β-CD, NS and RDP was prepared successfully, and the synergistic effect of P–NS with IFR in the flame retardation of PP was investigated. The results show that P–NS exhibited a distinct synergistic effect with IFR on FR PP. With a loading of 2.0 wt % P–NS (with the total content of additives kept at 25.0 wt %), the LOI value increased from 29.0 to 32.5%, the UL-94 rating was enhanced from V-1 to V-0, and PHRR decreased substantially from 343 to 235 kW/m^2. Simultaneously, THR, MLR, and av-HRR decreased dramatically. Finally, the morphology of the char residue of FR PP revealed that the synergistic effect between P–NS and IFR on the flame retardancy was due to the improvement in the formation of a compact and dense char barrier on the surface of the burning composites.

References

1. Lu, S. Y.; Hamerton, I. Prog Polym Sci 2002, 27, 1661.
2. Bourbigot, S.; Le Bras, M.; Duquesne, S.; Rochery, M. Macromol Mater Eng 2004, 289, 499.
3. Bugajny, M.; Le Bras, M.; Bourbigot, S. Fire Mater 1999, 23, 49.
4. Liu, Y.; Zhao, J.; Deng, C. L.; Chen, L.; Wang, D. Y.; Wang, Y. Z. Ind Eng Chem Res 2011, 50, 2047.
5. Huang, N. H.; Chen, Z. J.; Wang, J. Q.; Wei, P. Express Polym Lett 2010, 4, 743.
6. Ren, Q. A.; Zhang, Y.; Li, J. A.; Li, J. C. J Appl Polym Sci 2011, 120, 1225.
7. Ye, L.; Wu, Q. H.; Qu, B. J. J Appl Polym Sci 2010, 115, 3508.
8. Chen, X. L.; Jiao, C. M.; Wang, Y. Express Polym Lett 2009, 3, 359.
9. Wu, N.; Yang, R. J. Polym Adv Technol 2011, 22, 495.
10. Nie, S. B.; Hu, Y.; Song, L.; He, S. Q.; Yang, D. D. Polym Adv Technol 2008, 19, 489.
11. Bourbigot, S.; Le Bras, M.; Delobel, R.; Breant, P.; Tremillon, J. M. Polym Degrad Stab 1996, 54, 275.
12. Liu, Y.; Wang, J. S.; Deng, C. L.; Wang, D. Y.; Song, Y. P.; Wang, Y. Z. Polym Adv Technol 2010, 21, 789.
13. Tang, Y.; Hu, Y.; Wang, S. F.; Gui, Z.; Chen, Z. Y.; Fan, W. C. Polym Int 2003, 52, 1396.
14. Bright, D. A.; Dashevsky, S.; Moy, P.; Williams, B. J Vinyl Addit Technol 1997, 3, 170.
15. Pawlowski, K. H.; Schartel, B. Polym Degrad Stab 2008, 93, 657.
16. Huang, L.; Gerber, M.; Lu, J.; Tonelli, A. E. Polym Degrad Stab 2001, 71, 279.
17. Le Bras, M.; Bourbigot, S.; LeTallec, Y.; Laureyns, J. Polym Degrad Stab 1997, 56, 11.
18. Wang, H. F.; Li, B. Polym Adv Technol 2010, 21, 691.
19. Vyas, A.; Saraf, S.; Saraf, S. J Inclusion Phenom Macro 2008, 62, 23.
20. Uekama, K.; Hirayama, F.; Irie, T. Chem Rev 1998, 98, 2045.
21. Trotta, F.; Cavalli, R. Compos Interfaces 2009, 16, 39.

22. Swaminathan, S.; Pastero, L.; Serpe, L.; Trotta, F.; Vavia, P.; Aquilano, D.; Trotta, M.; Zara, G.; Cavalli, R. Eur J Pharm Biopharm 2010, 74, 193.
23. Alongi, J.; Poskovic, M.; Frache, A.; Trotta, F. Polym Degrad Stab 2010, 95, 2093.
24. Wei, M.; Shuai, X. T.; Tonelli, A. E. Biomacromolecules 2003, 4, 783.
25. Shuai, X. T.; Porbeni, F. E.; Wei, M. I.; Shin, D.; Tonelli, A. E. Macromolecules 2001, 34, 7355.
26. Ponchel, A.; Abramson, S.; Quartararo, J.; Bormann, D.; Barbaux, Y.; Monflier, E. Micropor Mesopor Mater 2004, 75, 261.
27. Chiu, Y. C.; Tsai, H. C.; Chou, I. C.; Li, S. M.; Ma, C. C. M. J Appl Polym Sci 2010, 118, 2165.
28. Pack, S.; Kashiwagi, T.; Cao, C. H.; Korach, C. S.; Lewin, M.; Rafailovich, M. H. Macromolecules 2010, 43, 5338.
29. Lee, K.; Yoon, K.; Kim, J.; Bae, J.; Yang, J.; Hong, S. Polym Degrad Stab 2003, 81, 173.
30. Pawlowski, K. H.; Schartel, B. Polym Int 2007, 56, 1404.
31. Li, J.; Wei, P.; Li, L. K.; Qian, Y.; Wang, C.; Huang, N. H. Fire Mater 2011, 35, 83.
32. Schartel, B.; Hull, T. R. Fire Mater 2007, 31, 327.
33. Wang, D. Y.; Liu, Y.; Wang, Y. Z.; Artiles, C. P.; Hull, T. R.; Price, D. Polym Degrad Stab 2007, 92, 1592.
34. Lu, H. D.; Wilkie, C. A. Polym Adv Technol 2011, 22, 14.
35. Jiao, Y. H.; Wang, X. L.; Wang, Y. Z.; Wang, D. Y.; Zhai, Y. L.; Lin, J. S. J Macromol Sci Phys 2009, 48, 889.
36. Dang, X. R.; Bai, X.; Zhang, Y. J Appl Polym Sci 2011, 119, 2730.